Peptide-conjugated MRI probe targeted to Netrin-1, a novel metastatic breast cancer biomarker

Clémentine Moreau, Tea Lukačević, Agnès Pallier, Julien Sobilo, Samia Aci-Sèche, Norbert Garnier, Sandra Même, Éva Tóth, Sara Lacerda

Peptide-Conjugated MRI Probe Targeted to Netrin-1, a Novel Metastatic Breast Cancer Biomarker

Clémentine Moreau,[1] Tea Lukačević,[1] Agnès Pallier,[1] Julien Sobilo,[2] Samia Aci-Sèche,[3] Norbert Garnier,[1] Sandra Même,[1] Éva Tóth,[*,1] Sara Lacerda[*,1]

[1] Centre de Biophysique Moléculaire, CNRS UPR4301, Université d'Orléans, Rue Charles Sadron, 45071 Orléans Cedex 2, France

[2] TAAM-In vivo Imaging Centre, MO2VING, CNRS UAR44, F-45071 Orléans 2, France

[3] Institut de Chimie Organique et Analytique, UMR CNRS-Université d'Orléans 7311, Université d'Orléans BP 6759, 45067, Orléans Cedex 2, France

Email : eva.jakabtoth@cnrs.fr ; sara.lacerda@cnrs.fr

Abstract

Despite significant progress in cancer imaging and treatment over the years, early diagnosis and metastasis detection remains a challenge. Molecular magnetic resonance imaging (MRI), with its high resolution, can be well adapted to fulfil this need, requiring the design of contrast agents which target specific tumor biomarkers. Netrin-1 is an extracellular protein overexpressed in metastatic breast cancer, implicated in tumor progression and appearance of metastasis. This study focuses on the design and preclinical evaluation of a novel Netrin-1 specific peptide-based MRI probe, GdDOTA-KKTHDAVR (Gd-K), to visualize metastatic breast cancer. The targeting peptide sequence was identified based on the X-ray structure of the complex between Netrin-1 and its transmembrane receptor DCC. Molecular docking simulations support the probe design. *In vitro* studies evidenced submicromolar affinity of Gd-K for Netrin-1 (K_d = 0.29 µM) and good MRI efficacy (proton relaxivity, r_1 = 4.75 $mM^{-1}s^{-1}$ at 9.4 T, 37°C). *In vivo* MRI studies in a murine model of triple-negative metastatic breast cancer revealed successful tumor visualization at earlier tumor development (smaller tumor volume). Excellent signal enhancement, 120 % at 2 min and 70% up to 35 min post injection, was achieved (0.2 mmol/kg injected dose), representing a reasonable imaging time window and a superior contrast enhancement in the tumor as compared to Dotarem injection.

Key Words

Targeted contrast agent; Netrin-1; MRI; Metastatic breast cancer; Biomarker; Early detection

Introduction

Cancer is a major debilitating disease affecting millions of people worldwide. In most cases, primary tumors can be successfully treated with surgical resection and adjuvant therapy, whereas metastatic cancer is the primary cause of morbidity and mortality, responsible for more than 90% of cancer deaths.[1] The molecular and cellular mechanisms of metastasis are constantly explored, but efficient treatment and imaging of metastatic cells remain a clinical challenge. Despite advanced screening technology available nowadays, most current clinical imaging agents lack specificity. Differential and accurate diagnosis is usually achieved in more advanced disease stages, limiting time for therapeutic care.

In oncology today, positron emission tomography (PET) based on elevated fluorodeoxyglucose (^{18}F-FDG) uptake in tumors is the major whole-body imaging modality used for initial staging, monitoring tumor proliferation and metastasis, and assessment of therapeutic responses. Nevertheless, ^{18}F-FDG is not specific for cancer as high metabolic rate can be associated to other etiologies (e.g. inflammation). Emerging methods relevant to cancer in PET imaging include monitoring cellular proliferation, tumor hypoxia, apoptosis, amino acid or cell membrane metabolism, imaging of tumor receptors and other tumor-specific gene products.[2, 3]

Magnetic resonance imaging (MRI) is a non-invasive, non-ionizing, powerful technique whose greatest advantage is high spatial and temporal resolution; it is largely available in the clinic, and more economic for both the health system and the patient. The lack of MRI sensitivity can be compensated by the use of contrast agents. The identification of viable molecular biomarkers accessible in MRI-detectable concentrations (typically >10 μM) sustains a major scientific challenge. Despite important progress in targeted molecular MR imaging probe development over the last decades, their *in vivo* translation is still scarce, with a single probe reaching clinical application (Vasovist®).[4] Examples of MRI detection of metastatic cancer by visualizing specific biomarkers are highly limited. For metastatic breast cancer for instance, to the best of our knowledge, solely two examples have been reported, both based on the targeting of fibronectin, an extracellular protein overexpressed in tumors.[5-7]

Netrin-1 is a multifunctional extracellular protein that regulates cell migration, cell adhesion, angiogenesis, apoptosis, suppression of inflammation, cell survival, tumorigenesis, and vascular endothelial cell function.[8-11] These activities are mediated by Netrin-dependent transmembrane receptors, DCC and UNC5b, exerting chemoattraction and chemorepulsion effects, respectively. In the absence of Netrin-1, these receptors induce cell death. The receptor/Netrin-1 interaction is crucial for cell migration and defines pro-invasive tumor activity. Tumor cells tend to develop autocrine Netrin-1 expression that blocks the receptors, inhibiting apoptosis, hence inducing tumor progression. Netrin-1 is upregulated in more than 60% of metastatic breast cancer, 47% of lung cancer, 38% of neuroblastoma and a large fraction of pancreatic cancer.[8] The involvement of Netrin-1 in the spread of cancer cells was further supported by the overexpression of Netrin-1 in metastatic breast carcinomas, as compared to their non-metastatic counterparts.[12, 13]

Netrin-1 overexpression observed in aggressive cancers makes this protein interesting as a biomarker for the development of imaging probes to assess aggressiveness and to distinguish metastatic over non-metastatic breast cancers. With Netrin-1's involvement in several biological processes related to tumor progression, angiogenesis and metastasis, we anticipate high local expression, potentially allowing for MRI detection of this protein with higher signal in tumor sites. Although released by tumor cells, Netrin-1 stays within the extracellular matrix, thus represents an accessible target around tumors cells.[13]

Mehlen and co-workers have used microbubbles functionalized with an anti-Netrin antibody for microbubble-based ultrasound imaging of breast cancer metastases.[14] Very recently, they have labelled the same antibody with ^{177}Lu for therapy, and showed tumor accumulation of their agent *via* SPECT imaging using the companion isotope ^{111}In.[13] While these studies have validated Netrin-1 as a viable biomarker of metastatic cancer, there remains a clear need for the development of higher resolution imaging methods. Although ultrasound is commonly used in the clinic, it lacks the depth and resolution necessary for an accurate detection of more spread and remote metastases. SPECT requires the use of a radionuclide and it is less available and more costly for patient assessment than MRI.

Compared with protein- or antibody-based imaging probes, small molecular agents have advantageous clinical translation potential, including the ease of characterization, structural optimization, and favorable pharmacokinetic properties. In particular, molecular imaging probes containing small peptides for biological recognition can provide comparable targeting capabilities as full proteins.[2] Herein we propose a novel peptide-based MRI contrast agent consisting of a DOTA-like chelator conjugated to a small peptide which recognizes Netrin-1. The peptide sequence selected as targeting moiety was identified thanks to the X-ray structure of the Netrin-1/DCC complex reported in the literature.[15] Docking studies were performed to prove that the conjugation of a Gd-DOTA to the peptide does not perturb its binding to Netrin-1. Complexation of the chelator with Gd^{3+} has allowed for MRI detection, while analogues with other metal ions, such as Eu^{3+} or $^{111}In^{3+}$ have enabled *in vitro* characterization and *in vivo* validation. *In vivo* MRI in a murine model, complemented by *ex vivo* biodistribution studies, has evidenced the superior imaging performance of this novel peptide-based Netrin-1 targeted probe to visualize metastatic breast cancer as compared with the MRI gold standard contrast agent Dotarem® (Gd-DOTA).

Results and Discussion

Probe design

The Netrin-1-specific targeting moiety has been identified based on the analysis of the amino acid residues in the binding epitope of Netrin-1, centered around Pro320, to its receptor DCC (residues 856 to 861 of DCC), as previously reported in the literature.[15] The small sequence selected, KTHDAVR, was then conjugated to a DOTA-monoamide metal chelator via the N-terminus by adding an extra lysine, thus providing DOTA-KKTHDAVR (K). For the *in vitro* characterization of the binding properties of the peptide sequence, a TAMRA (5-carboxytetramethyl rhodamine) labeled KKTHDAVR derivative (Rho-K) was also designed. Both compounds were custom-synthesized by Peptide Synthetics Ltd (Hampshire, UK). Figure 1 shows the design strategy and the structure of the probes.

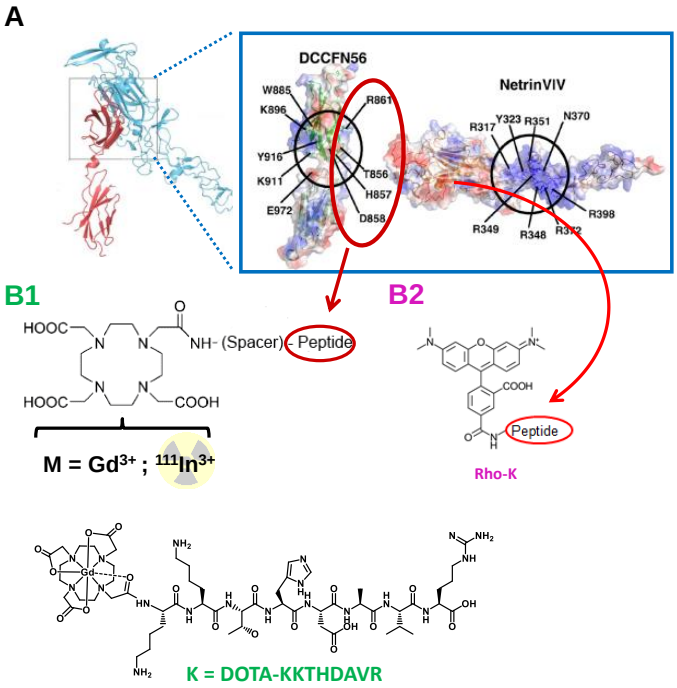

Figure 1: Schematic representation of the selection of the small peptidic targeting moiety (A) and of the structure of the DOTA (B1) and TAMRA (B2) derivatives.

For the conjugation of a bifunctional chelate to a biomolecule, several methods are available. The most current one involves the activation of a carboxylic group of the chelate which will then react with an amino group, usually of a lysine, present in the biomolecule (e.g. antibody or a peptide).[16, 17] Herein, the peptide conjugation was performed *via* solid support and DO3A^{TBu} or TAMRA were added and allowed to react as "extra amino acid" residues via the formation of an amide bond between the COOH group of the chelate or TAMRA and the N-terminus amine of the peptide. The protecting groups are then removed along with the cleavage of the peptide from the solid support, and the product is purified by HPLC using an acetonitrile/water eluent containing 0.1 % Ammonium Acetate (pH 8.5), prior to lyophilization. All compounds are kept at -20°C and restored in PBS before use. Figures S1-S2 show the HPLC chromatogram and mass spectra of K and Rho-K.

In vitro binding affinity

In vitro affinity towards Netrin-1 (commercially available human recombinant Netrin-1) and control proteins (human serum albumin (HSA), and two major extracellular matrix proteins: type I collagen and laminin, a noncollagenous netrin-family related[10] protein) was assessed by fluorescence studies. For this, each protein was immobilized in a 96-well plate and incubated with solutions of different concentrations of Rho-K (50 nM to 130 µM, n=3). After 2 h incubation at room temperature, the fluorescence intensity was measured ($\lambda_{exc/em}$=540/580 nm). To verify that the conjugation of the metal complex does not affect the affinity of the small peptide sequence, we also studied the Eu^{3+} complex of K, chemical analogue of Gd-K. We have used a "DELFIA-like" assay (Dissociation-Enhanced Lanthanide FluoroImmunoAssays), similarly to previous reports[18-21], where following protein immobilization and probe incubation (2h incubation, 50 nM to 10 µM, n=3), the unbound Eu-K solution is removed, the plate well washed with PBS and DELFIA-Enhancement Solution® is added and allowed to react for 30 min. The DELFIA-Enhancement Solution® acts as a sensibilization agent for the Eu^{3+} luminescence. The time-resolved fluorescence of the plates is then measured ($\lambda_{exc/em}$=340/615 nm). Similar affinity

studies with Eu-DOTA without the peptide sequence were performed as negative control; in these assays the "bound" luminescence intensity was very low, preventing data fitting. To determine dissociation constants (K_D; Table 1), data obtained *via* both methods (Figure S3) were fitted using an imbedded model for one specific binding site of GraphPad Prism v7.05.

Table 1: *In vitro* binding affinity (dissociation constants, K_D; mean ± SD, n=3) towards different proteins, and comparison with previously reported targeted MRI probes.

	K_D (µM)					
Protein	**Rho-K[a]**	**Eu-K (DELFIA)[b]**	**Vasovist[c]**	**EP-2104R[d]**	**CREKA-tris(Gd-DOTA)$_3$[e]**	**ZD2-Gd(HP-DO3A)[f]**
Netrin-1	0.29 ± 0.09	1.2 ± 0.4				
HSA	112 ± 22	no fit	80			
Coll I	14 ± 2	29 ± 7				
Laminin	2.1 ± 0.4	---				
Fibronectin	---	---			6.0	3.2
Fibrin	---	---		1.7		

[a] direct method; [b] indirect method (DELFIA); [c] ref [22]; [d] ref [23]; [e] ref [24]; [f] ref [6].

The dissociation constants are in the µM range for the interaction of Rho-K and Eu-K with Netrin-1, although a slightly higher K_D is obtained for Eu-K with the "indirect" method DELFIA. These affinities are similar to those reported for targeted MRI probes, such as the HSA-specific Vasovist® which was in clinical use, and EP-2104R, a fibrin-specific probe that reached clinical trials. This shows that the Netrin-1 affinity of our probe might be compatible with MRI detection. The affinity differences towards the different proteins were further visualized by plotting the fractional occupancy[25], i.e. percentage of the ligand that is bound to a protein for a given concentration (Figure 2, see ESI for calculations), which illustrates superior binding to Netrin-1.

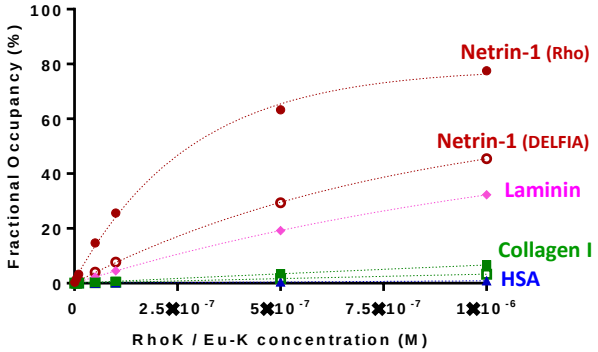

Figure 2: Fractional occupancy of Rho-K for target Netrin-1 (●), and control proteins laminin (◆), type I collagen (■) or HSA (▲), and of Eu-K for Netrin-1 (○).

Docking Studies

To better understand the structural organization of the complex formed between Netrin-1 and the peptide sequence used for targeting, we first carried out a docking experiment in triplicate with AutoDock CranckPep[26] by varying the initial peptide conformation. We observed three very similar conformations for the best pose of the three runs (Figure 3A). The peptide is docked in a large groove at the protein surface, giving sufficient space to accommodate the Gd-DOTA moiety (Figure S4). The coordinates of Gd-DOTA have been extracted from a

deposited structure in the RCSB PDB (PDB ID 1NC4) and manually grafted at the *N*-terminal position of the peptide (Figure 3B). This Gd-K - Netrin-1 system has then been submitted to 500 ns of molecular dynamics simulation at 300K in order to investigate the behavior of the Gd-DOTA moiety and its impact on the peptide-Netrin-1 interaction. We observed an evolution of the peptide conformation associated to an energetical stabilization of the Gd-K - Netrin-1 interaction during the last 300 ns of the simulation (Figure S5). During the simulation, the Gd-DOTA moiety is solvent-exposed and free to move on the surface of the protein, without disturbing the peptide-Netrin-1 interaction.

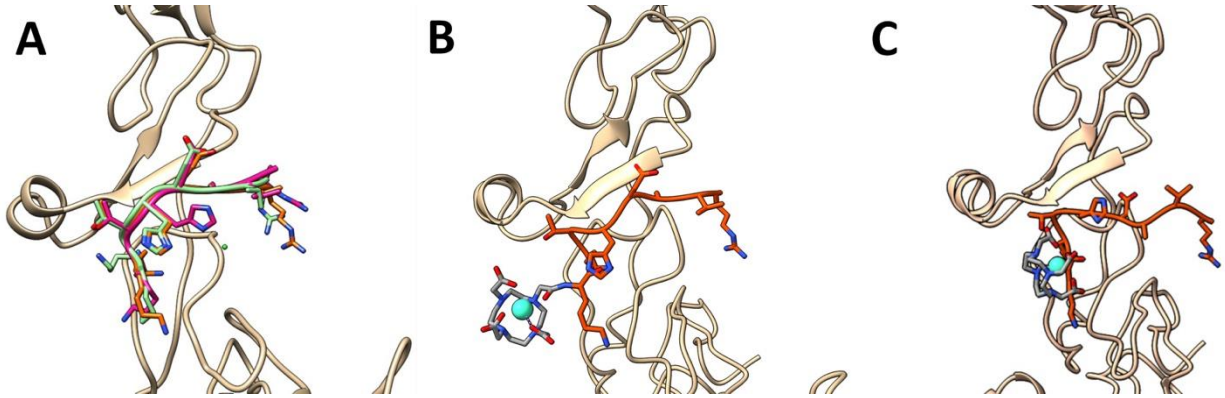

Figure 3: 3D representation of the molecular modeling results. The Netrin-1 structure is represented as beige ribbon. A) Representation in licorice and ribbon of the best pose of the peptide docked on the Netrin-1 structure (PDB ID 4URT) from 3 runs (in orange, green and magenta respectively), B) Position of the Gd-DOTA moiety (in grey licorice, Gd is represented as cyan sphere) manually docked on the peptide best pose (orange), C) Stabilized conformation obtained during the 500 ns of molecular dynamics simulation.

Relaxivity measurements

To evaluate the MRI efficacy of Gd-K, field dependent relaxivities (NMRD profiles) of Gd-K and Dotarem® were measured at 25°C and 37°C (Figure 4A; NMRD = Nuclear Magnetic Relaxation Dispersion).

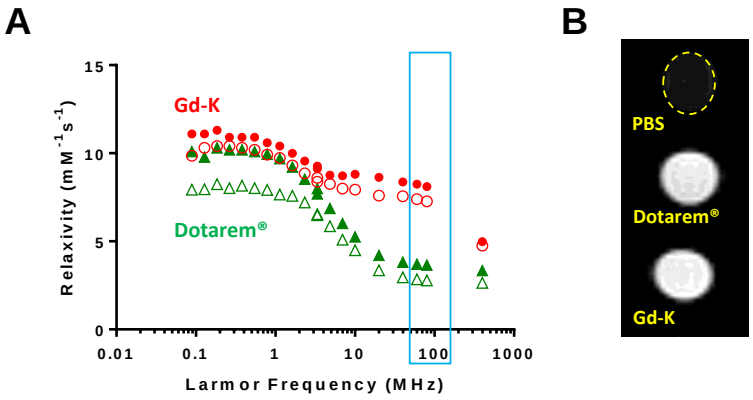

Figure 4: (A) NMRD profiles of Dotarem® (green triangles) and Gd-K (red spheres) at 25 °C (closed symbols) and 37 °C (open symbols); the blue rectangle indicates the clinical magnetic field range. (B) T_1-weighted images at 9.4 T of phantom tubes containing phosphate-buffered saline (PBS), Dotarem® (1.60 mM) and Gd-K (1.14 mM).

The relaxivity of Gd-K is higher than that of Dotarem® (Gd-DOTA), with a remarkable difference at clinical fields (blue rectangle in Figure 4A). This certainly results from the higher molecular weight, thus slower rotation of Gd-K, which has major impact between 20-100 MHz.[27] Second-sphere water molecules around the peptide chain can further contribute to the higher relaxivity. Significant aggregation could be excluded by concentration-dependent relaxivity measurements of Gd-K (0.5 to 2.4 mM) which showed practically no variation. MRI phantom images at 9.4 T (Figure 4B) are consistent with the better relaxation efficacy of Gd-K. Relaxivities were also determined in the phantom solutions, using the R_1 of PBS as diamagnetic contribution (r_1=4.93 and 3.83 $mM^{-1}s^{-1}$ for Gd-K and Dotarem®, respectively, at room temperature).

In vivo MRI studies

Perfusion studies for tumor characterization

Tumors were induced in female mice by injecting 10^6 4T1 cells, for which overexpression of Netrin-1 has been previously confirmed (courtesy of Drs B. Gibert and P. Mehlen, Lyon). This tumor type has been extensively characterized in both terms of its Netrin-1 expression and general tumor development, and it was shown that these tumors lead to the appearance of metastasis. Although in our protocol we did not follow the formation of metastasis, we assume similar tumorigenesis and metastatic development, as described by Mehlen and co-workers, who kindly provided the 4T1 cells used for tumor induction.[12, 13] As these 4T1 tumors grow rather fast and typically become necrotic, tumor permeability is certainly compromised.[28, 29] To identify the imaging window within tumor evolution best adapted for the validation of our probe, we have first performed an MRI perfusion study using intravenous injection of Dotarem® (0.2 mmol/kg). For this, we followed a group of 5 tumor-bearing mice over time, between days 4 and 12 post induction (p.ind.) of the tumor. Signal intensity in the tumor and the aorta over time, post injection of Dotarem® allowed us to assess the extravasation of the contrast agent in the tumor, *via* the parameters K_{trans} (volume transfer constant between the intravascular and the extravascular extracellular space, related to tumor permeability), and Vp (plasmatic volume of the tumor).[30]

We analyzed the evolution of the signal enhancement with the tumor growth over 12 days by placing a ROI in the tumor core (see figure S6 for a representative example), and the calculated parameters (K_{trans} and Vp) are depicted in Figure 5 as a function of post tumor induction time.

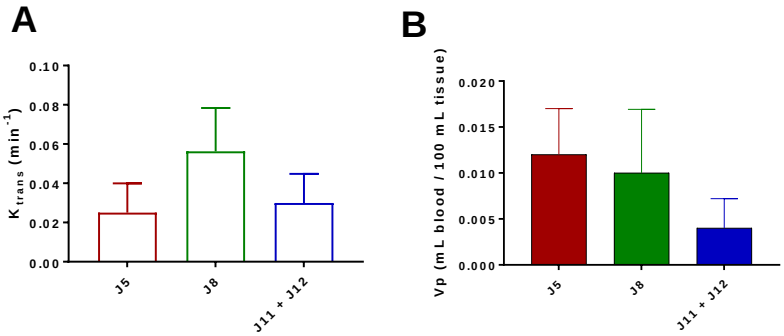

Figure 5: Perfusion parameters, K_{trans} (A) and Vp (B), based on Dotarem® distribution by post induction time. Data are presented in mean±SD (n=5).

Despite that the dispersity of tumor growth yields rather large standard deviation of the parameters, the K_{trans} values found are within the range of reported literature data for the same 4T1 breast cancer model. In these 4T1 tumor-bearing mice, an increase of K_{trans}, was related to better vascularity induced by tumor treatment. Nevertheless, K_{trans} changes did not always reflect tumor size change.[31, 32] The majority of previous studies agree that the periphery of the tumor has higher permeability than its core, in agreement with a necrotic behavior. Here, we also observe enhanced contrast in the periphery, as a result of higher contrast agent uptake (Figure S6A). K_{trans} peaks at day 8 p.ind., then decreases. In parallel, the tumor plasmatic volume (Vp) decreases continuously. Altogether, these results indicate that early p.ind. timepoints (up to day 8) correspond in general to better tumor permeability and might be favorable for the evaluation of the new probe.

In vivo MR imaging with Gd-K

We have thus decided to image mice using our novel probe at days 4 and 8 post induction of the tumor. For this, we have induced another group of mice with 10^6 4T1 cells, and injected each mouse at days 4 and 8 post induction with 0.2 mmol/kg of Gd-K (intravenous injection, tail vein). T1-weighted images were acquired before and up to 75 min post injection, at 9.4T, and the percentage of MRI signal enhancement was plotted (Figure 6). Figure S7 depicts the ROI selected for determination of signal enhancement at the highest intensity images.

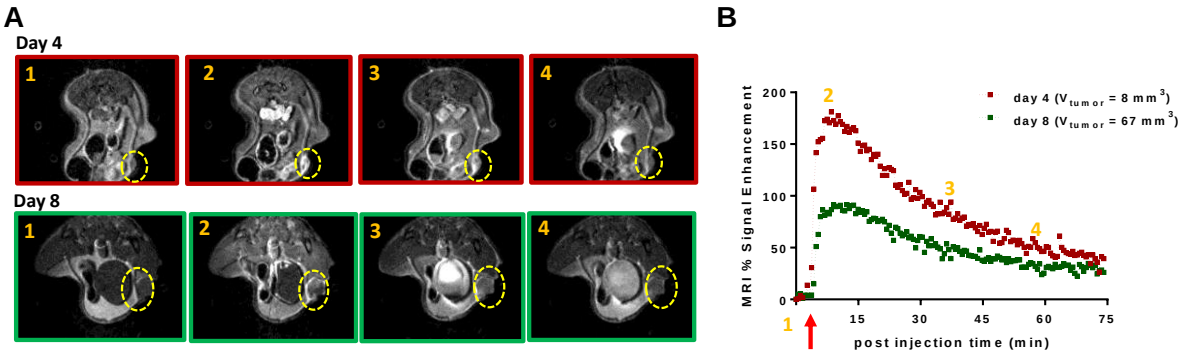

Figure 6: (A) T1-weighted MR images at 0 min (1), 2 min (2), 35 min (3) and 60 min (4) post injection of a representative mouse scanned at days 4 and 8 post induction. The yellow circle indicates the tumor location. (B) Signal enhancement profiles up to 75 minutes post administration of Gd-K – the red arrow indicates the injection of the contrast agent.

Figure 6 evidences a clear uptake of Gd-K in the tumor core at day 4 (8 mm^3 volume for the selected animal), which becomes restricted to the tumor periphery at day 8 (67 mm^3), in agreement with the necrotic core and lower vascularization of this larger tumor. Tumor to muscle comparison reveals higher tumor signal enhancement and shows that the muscle uptake does not very with tumor evolution (figure S8, see figure S7 for ROI selection).

Tumor development was found quite disperse within the groups, despite the same number of cells used for tumor induction. Therefore, we have defined mice groups by tumor volume range for a better comparison between the mice imaged either with Gd-K or with Dotarem® (Figure 7). Tumor volumes were determined from the MR images, and the groups were defined as: V_{tumor}=0-50 mm^3 (n=2; n=5 for Dotarem® and Gd-K injection, respectively), 50-100 mm^3 (n=7; n=2) and 100-200 mm^3 (n=2; n=2).

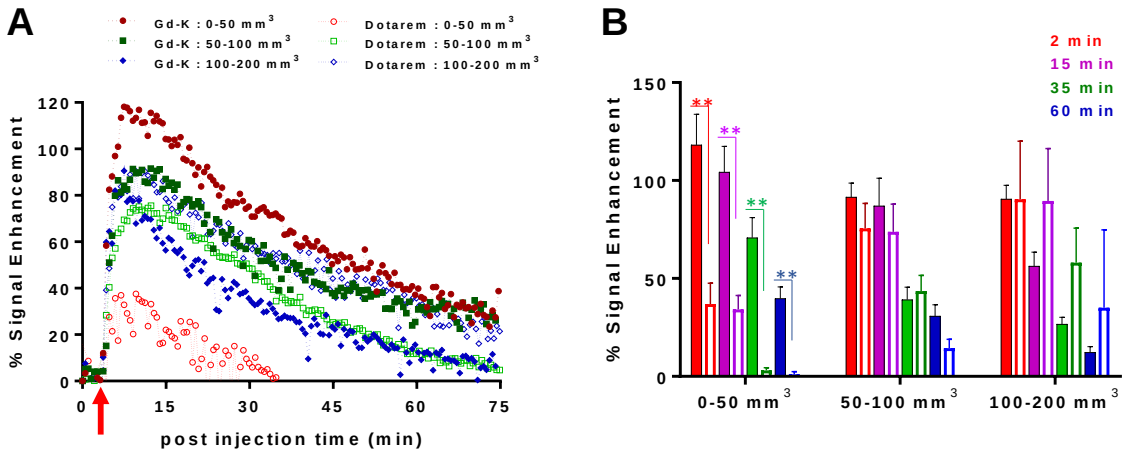

Figure 7: (A) MRI signal enhancement profile by tumor volume range (0-50, 50-100 and 100-200 mm^3) for all animals, up to 75 minutes post administration of Gd-K (full symbols) or Dotarem® (open symbols) – the red arrow indicates contrast agent injection. Error bars have been removed for better visibility. (B) Percentage of signal enhancement at different post injection times (2, 15, 35 and 60 min) for Gd-K (full bars) and Dotarem® (empty bars; mean ±SEM). For 0-50 mm^3 tumors, differences between Gd-K and Dotarem® injections are significative at all times post injection (p = 0.0092; 0.0055; 0.0028 and 0.0027, respectively).

For small tumors (0-50 mm^3 volume), Gd-K induces unambiguously superior signal intensity as compared to Dotarem®, at any post injection timepoint (e.g. threefold higher signal intensity at 2 min p.i.), which can be particularly important for early diagnosis, while for larger tumors, the superiority of Gd-K vanishes (figure 7B). The results indicate remarkable tumor visualization with Gd-K at earlier tumor development (smaller volume), with excellent signal enhancement, 120 % at 2 min and 70% up to 35 min p.i., representing a reasonable imaging time window. To the best of our knowledge, this constitutes the first MR imaging study using a probe specific of the metastatic biomarker Netrin-1.

For the same breast cancer murine model, two peptide-based molecular MRI probes, targeting fibronectin, were reported to detect tumors and metastases. CREKA-tris(Gd-DOTA)$_3$ consists of three Gd-DOTA conjugated to a 5-residue peptide (K_D = 6 µM; r_1 = 22 $mM^{-1}s^{-1}$ per molecule at 64 MHz).[5] At an injected dose identical to ours (0.2 mmol/kg), tumors of <19 mm^3 volume could be detected, with 76–122 % signal enhancement (7 T). Considering that we achieve similar signal enhancement with Gd-K which has four-fold lower relaxivity in its unbound form, and that the “in vivo Netrin-1 bound form” of our agent is expected to have a higher relaxivity, our Netrin-specific agent looks very promising. The second fibronectin-targeted probe, ZD2-Gd(HP-DO3A) contains a 7-residue peptide (K_D = 3.2 µM; r_1 = 5.44 $mM^{-1}s^{-1}$ at 128 MHz).[6] The authors reported 150% signal enhancement at 10 min post injection (0.1 mmol/kg dose, 7 T) for tumors which were induced with a 3-fold higher number of cells per mouse and imaged 3 weeks later, thus the tumors were certainly bigger than in our case which makes direct comparison more difficult. In overall, Gd-K shows excellent signal enhancement in small, early-stage tumors, and performs clearly better than the MRI gold standard Dotarem®.

Ex vivo biodistribution studies

To further evaluate the biodistribution of the novel imaging probe, the Indium-111 analogue was synthesized and injected in breast tumor-bearing mice (vol = 60±10 mm^3) induced with

cells overexpressing Netrin-1 (4T1 cells) or cells weakly expressing Netrin-1 (MDA-MB-231). Netrin-1 mRNA and protein expression between different breast tumor models were previously compared in the literature, though without exact quantification. Within the 48 human breast and 2 mouse mammary cell lines studied, 4T1 tumor cells were the ones expressing the highest amount of Netrin-1, while in MDA-MB-231 cells the protein was barely detectable.[12]

For comparison, ^{111}In-DOTA biodistribution (Dotarem® analogue) was studied in 4T1 tumor bearing mice under the same conditions.

These studies consist in the intravenous injection of the probe, sacrifice of the animals at a short (15 min) and a longer (4h) post-injection time (n=3 per time point), and harvesting of the tumors as well as relevant organs for quantification of the ^{111}In activity. Such biodistribution allows for assessing target accumulation and elimination pathways. It can potentially indicate in vivo ^{111}In release from the probe, giving information about probe stability.

^{111}In-K and ^{111}In-DOTA were obtained with >98% radiochemical yield by reacting ligand solutions with $^{111}InCl_3$ for 1h at 90°C and pH 5 (acetate buffer). Mice (n=3) were injected intravenously in the tail vein (≈2.5 MBq/mouse) and sacrificed at 15 min and 4h post injection. The biodistribution data, expressed in percentage of injected dose per gram of tissue (%ID/g ± SEM), are presented in Figure 8A, Figure S9 and Tables S1 and S2.

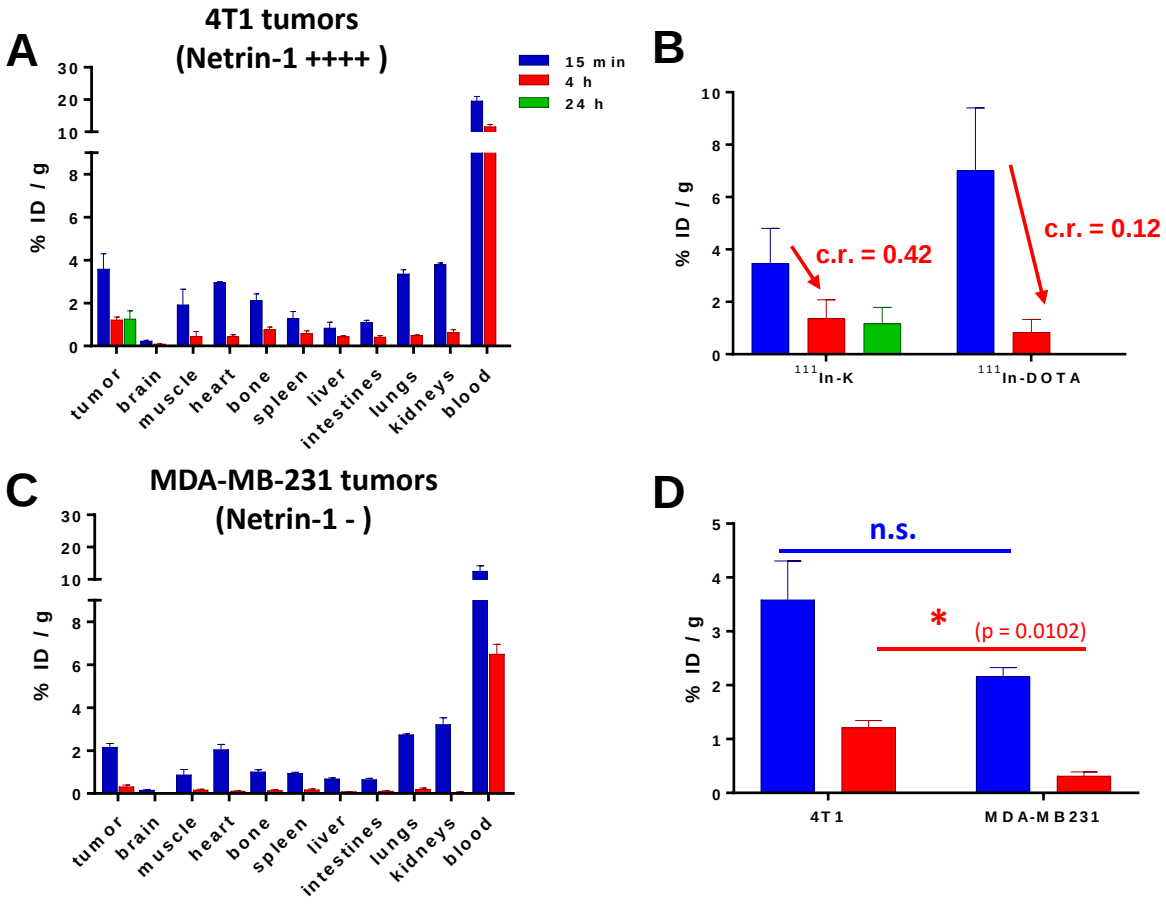

Figure 8: (A) Biodistribution profile at 15 min, 4 h and 24 h post intravenous injection of ^{111}In-K in 4T1 tumor-bearing mice. (B) Comparison of tumor uptake for ^{111}In-K and ^{111}In-DOTA at different time points with indication of clearance ratio (c.r. = uptake at 4h / uptake at 15 min) between 15 min and 4 h. (C) Biodistribution profile at 15 min, 4 h and 24 h post intravenous injection of ^{111}In-K in MDA-MB-231 tumor-bearing mice. (D) Comparison of tumor uptake of ^{111}In-K in overexpressing Netrin-1 (4T1 cells) or cells

weakly expressing Netrin-1 (MDA-MB-231) at 15 min and 4 h post injection. Data are expressed in percentage of injected dose per gram of tissue (%ID/g ± SEM; n = 3).

Both radiocomplexes show fast renal clearance and no specific organ retention, except for ^{111}In-K in the 4T1 tumor which is the only localization where ^{111}In is detectable even 24 h p.i. The low bone and muscle uptakes at 4h p.i. reveal good *in vivo* stability for both complexes and exclude potential transmetalation, in accordance with the high stability and inertness of In^{3+}-DOTA-derivatives. “Free” ^{111}In uptake would indeed occur mainly in bone and muscle, with reported values 25- to 200-fold higher at 6h p.i., respectively,[33] than those of ^{111}In-K and ^{111}In-DOTA. Also, TLC of a blood sample collected at 4h p.i. indicates good *in vivo* stability of ^{111}In-K (>95%, Figure S10).

Importantly, ^{111}In-K and ^{111}In-DOTA have very different tumor clearance. While early uptake is higher for ^{111}In-DOTA (3.6±0.7 %ID/g and 6.6±1.3 %ID/g at 15 min p.i. for ^{111}In-K and ^{111}In-DOTA, respectively), at 4h, the ratio is inversed and at 24h 1.3±0.4 %ID/g ^{111}In-K is still present in tumors, while ^{111}In-DOTA is eliminated (figure 8B). The slower tumor elimination of ^{111}In-K is promising and in accordance with the MRI findings.

Notably, we can observe important differences when comparing the tumor uptake values of ^{111}In-K in MDA-MB-231 and 4T1 tumors, with weak and high Netrin-1 expression, respectively (figure 8D). At both time points, the uptake is superior for the 4T1 tumors. This difference is particularly important at 4 h p.i., with a fourfold higher retention of ^{111}In-K in the Netrin-1 expressing tumor (0.32±0.08 *vs* 1.2±0.1 %ID/g, p=0.0102). The clearance ratio is also different for the two tumor types. For the tumors poorly expressing Netrin-1, it is 0.15 for ^{111}In-K and 0.16 for ^{111}In-DOTA. These values are also close to the one determined for ^{111}In-DOTA in 4T1 tumors, all showing non-specific tumor retention. In contrast, the clearance ratio of ^{111}In-K in 4T1 tumors is much higher, 0.42, reflecting specific uptake. These facts all advocate in favor of in vivo specific targeting of our novel probe towards Netrin-1.

The recently reported ^{111}In-NOTAGA-NP137, an antibody-based probe targeted to Netrin-1, allowed SPECT detection of tumors of 100-200 mm^3, with an accumulation of 14% at 48 h p.i. However, liver and spleen accumulation was also observed, with uptakes of ~10 %ID/g (48h p.i.), indicative of slower elimination.[13] While such slower accumulation is desirable for therapy, imaging sessions preferably take place shortly after patient injection. Thus, probes with faster uptake and elimination, such as for ^{111}In-K, are advantageous.

Conclusion

We have successfully developed an MRI probe for the potential detection of Netrin-1, an emerging biomarker in metastatic breast cancer. The peptide-based agent Gd-K possesses good relaxivity at clinically relevant magnetic fields and submicromolar *in vitro* affinity for Netrin-1. *In vivo* studies in tumor-bearing mice indicate promising tumor uptake and renal elimination. In early-stage, small tumors, Gd-K provides significantly better MRI signal enhancement than the MRI gold standard Dotarem®, in a reasonable time window.

Experimental Procedures (Materials and Methods)

Materials

$GdCl_3 \cdot 6H_2O$, $EuCl_3 \cdot H_2O$, PBS (Dulbecco′s Phosphate Buffered Saline, pH 7.4), Multielement solution 1 for ICP, HNO_3, xylenol orange, and human serum albumin were purchased from Sigma-Aldrich and Dotarem® from Guerbet, France. Recombinant human Netrin-1 protein was purchased from Bio-techne. Mouse laminin and bovine type I collagen were purchased from Corning BV. DELFIA Enhancement Solution® was purchased from Perkin Elmer. All products were used without further purification.

Synthesis of the lanthanide (Ln^{3+}) complexes

Lanthanide (Ln^{3+}) complexes were prepared by mixing an aqueous solution of DOTA-peptide with stoichiometric amounts of chosen $LnCl_3 \cdot xH_2O$. The pH of the reaction mixture was continuously adjusted to 6-7 with aqueous NaOH. The solutions were left stirring overnight at room temperature. After confirming the absence of free lanthanide by xylenol orange test,[34] the solutions were freeze dried and stored at -20 °C. Lanthanide complexes were restored in PBS 10 mM prior to use.

Binding assays

Fluorescence-based DELFIA binding assays (Dissociation-enhanced lanthanide fluoroimmunoassays) were performed using the analogue Europium (Eu^{3+}) complex of DOTA-peptide (Eu-K). Briefly, 96-well flat bottom plates (Yellow Plates, Perkin Elmer) were coated overnight with proteins of interest (100 µl/well, 50 µg/ml), here Netrin-1, human serum albumin (HSA), laminin and type I collagen. Different complex concentrations were incubated for two hours at room temperature, the incubation solutions were removed, and the coated wells washed with PBS. A further 30 min incubation with DELFIA Enhancement solution® was performed after which time resolved fluorescence intensity was measured ($\lambda_{exc/em}$ = 340/615 nm). The concentrations used for each assay ranged from 50 nM to 10 µM and studies were performed in triplicates (n=3).

Binding assays using the TAMRA derivative (Rho-K) were also performed. Briefly, after coating the 96-well flat bottom plates with proteins of interest (Netrin-1, HSA, laminin and type I collagen), Rho-K was used to perform the binding assay. Different Rho-K concentrations were incubated for 2 h at room temperature, the incubation solution was removed and the coated wells washed with PBS. The fluorescence intensity was then measured ($\lambda_{exc/em}$ = 540/580 nm). The concentrations used for assay with Rho-K ranged from 50 nM to 130 µM. Studies were performed in triplicates (n=3).

Fluorescence intensity was measured on CLARIOstar Plus microplate reader (BMG Labtech, France). Data obtained was treated in GraphPad Prism v7.05 and the binding affinity constants (K_D) were determined based on a “one specific binding” model, imbedded in the program. Data are presented as mean±SEM (n=3).

Molecular modelling

Molecular docking

Docking experiments were performed by using the AutoDock CranckPep (ADCP) program with the following peptide sequence as input: kkthdavr. The structure of Netrin-1 in complex with FN5- FN6 of DCC (PDB ID 4URT) was chosen as target structure. After the removal of the DCC netrin receptor, the Netrin-1 structure was protonated and prepare for docking with the python scripts provided by the ADFRSuite.[35] As we noticed the presence of chlorine ion at the

interface of the two proteins in the structure of PDB ID 4URT, two structures were considered for the peptide docking: one by keeping the chlorine ion at the interface and another without this ion. 3 runs of docking were performed by varying the type of the initial conformation of the peptide and the structure of the receptor. Two runs were performed starting from a combination of 80% extended conformation and 20% helical conformation of the peptide against the structure with and without the chlorine ion at the interface. A third one was performed against the structure without the chlorine ion with a starting structure for the peptide generated by the PEP-FOLD server.[36, 37] The best model of each run was kept and compare to the others.

Probe grafting

The coordinates of the Gd-DOTA molecule have been extracted from the structure of the monoclonal antibody 2D12.5 Fab complexed with Gd-DOTA (PDB ID 1NC4) and manually grafted at the N-terminal position of the peptide with the help of the Chimera software[38].

Molecular dynamics simulations

Molecular dynamics simulations were performed with the pmemd code of the Amber 18 package.[39] The parameters of the Gd-DOTA were assigned by using the antechamber module of the AmberTools package and gaff forcefield.[40] For the Netrin-1 protein, the protonation state at a pH of 7.4 was assigned to the titratable residues using PROPKA.[41] The force field parameters were attributed to the protein using ff14SB.[42] The system was then solvated in a rectangular box with a buffer of 10 Å and with a TIP3P explicit water model, neutralized with 15 Cl- counterions and finally, 53 Na+ and 53 Cl− counterions were added to reach an ionic strength of 0.015 M. The system was energetically minimized with harmonic restraints applied on the interacting hydrogen bonds between the peptide and the Netrin-1, then heated to 300K. The system has then been equilibrated over a total duration of 4 ns by gradually relaxing the harmonic restraints. 500 ns of molecular dynamics production are thus performed on this equilibrated system.

Relaxometric measurements

Gd-K was characterized by relaxivity measurements in different media (PBS and in presence of 0.6 mM of HSA). Longitudinal relaxation rates have been recorded on a Stelar SMARtracer Fast Field Cycling NMR relaxometer (0.01 to 10 MHz) and a Bruker WP80 NMR electromagnet adapted to variable field measurements (20, 40, 60 and 80 MHz) and controlled by the SMARtracer PC-NMR console. The temperature was controlled by a VTC91 temperature control unit and maintained by a gas flow. Longitudinal relaxation rate was also recorded at 400 MHz on a Bruker Advance Spectrometer using a 5 mm BBFO probe in D_2O.

Gd^{3+} concentration was confirmed by Bulk Magnetic Susceptibility measurements (600 MHz, Bruker Advance Spectrometer, 5 mm BBFO probe in D_2O)[43] and/or ICP-OES.

ICP-OES measurements

ICP-OES measurements were performed with a Jobin Yvon ULTIMA2 Spectrometer (Longjumeau, France). Standard Ln solutions were prepared from a commercial Multielement solution 1 for ICP in 5 % HNO_3 matrix. Samples were digested in concentrated HNO_3 for 48 h at room temperature followed by 18 h at 65 °C. The resulting solutions were then diluted 1:13, to reach 5 % in HNO_3. Measurements were performed in triplicate, using the most accurate band for Gd (342.246 nm) yielding a calibration curve with R^2 of 0.9997.

MRI Phantoms

MR images of 3 tubes containing PBS, Dotarem® (0.5 mM) and Gd-K (0.514 mM) were acquired on a 9.4 T horizontal ultra-shielded superconducting magnet dedicated to small animal imaging (Bruker Biospin, Wissembourg, France) and equipped with a classical Bruker birdcage coil 35 mm inner diameter, and Paravision 5.0 software (Bruker BioSpin, Wissembourg). The T_1-weighted images were acquired using rapid spin echo sequence with TE = 10 ms and TR = 50, 100, 200, 400, 800, 1000, 1500 ms. The resolution is 46.8x46.8 μm^2. Slice thickness is 1.0 mm. T_1 values have been calculated using Paravision software.

Animal studies

8-weeks-old BALB/cByJRj and BALB/c Nude females were purchased from Janvier Labs (Le Genes Saint Isle, France). All animal experiments were carried out in accordance with the guidelines for animal experiments and under permission numbers 30867 (MRI) and 27037 & 43235 (biodistribution), from the French “Ministère de l’Enseignement Supérieur, de la Recherche et de l’Innovation”.

Cell culture and tumor induction

4T1 cells used in this work have been kindly provided by Dr Benjamin Gibert (Centre de Recherche en Cancérologie de Lyon, France). Netrin-1 overexpression in the cell line has been previously assessed.[12]

After thawing, the cells are cultured in StableCell™ RPMI-1640 cell media, in the presence of glutamine and sodium bicarbonate stabilizers, complemented with 10% fetal bovine serum and 1% penicillin and streptomycin. The cells were counted using a Malassez cell and Trypan blue and re-suspended in PBS.

Tumor inductions were performed by injecting $2.5x10^5$ (for biodistribution studies) or $1x10^6$ cells (for MRI studies) in 100 µL PBS, in the 4th right inguinal mammary.

MDA-MB-231-luc-D3H2LN cells used in this work have been purchased by Caliper Life Science (parental line source: MD Anderson Cancer Center, University of Texas). After thawing, the cells are cultured in StableCell™ DMEM High glucose cell media, in the presence of glutamax and sodium Pyruvate, complemented with 10% fetal bovine serum and 1% penicillin and streptomycin. The cells were counted using a Malassez cell and Trypan blue and re-suspended in PBS.

Tumor inductions were performed by injecting $2x10^6$ cells in 100 µL PBS, in the 4th right inguinal mammary for biodistribution studies.

MRI studies

1. **Perfusion studies**

Magnetic resonance acquisitions were performed on a 9.4 T horizontal ultra-shielded superconducting magnet dedicated to small animal imaging (Bruker Biospin, Wissembourg, France) and equipped with a classical Bruker birdcage coil 35 mm inner diameter. Animals were anesthetized by inhalation of 2% isoflurane then maintained during MR experiments at 1.5% (0.5 L/min mixed in air and oxygen with 1:1 ratio). The physiological body temperature was maintained inside the magnet by circulating warm water. A pressure sensor was used to monitor the respiration cycle and obtain the respiration frequency for the reconstruction of Ig-

FLASH (intra-gate fast low angle shot) sequence. The volume of the tumors can be assessed based on these images.

For tumor and organs localization, coronal images using a gradient echo (Ig-Flash) sequence with the following parameters: TE/TR = 4 ms/200 ms, flip angle=20°, FOV size = 3x3 cm, matrix size = 256*256, slice thickness = 1 mm, to display 117×117 μm^2 in plane resolution for a duration of 4 min (10 accumulations).

A T_1-weighted spin echo sequence (resolution 234×234 μm^2, TE/TR=21/125 ms) was set and an image was obtained each 32 seconds, for 1h30. The Dotarem® contrast agent was manually injected (100 µL; 0.2 mmol/kg) 4 min after the beginning of the acquisition via a catheter placed in the caudal vein. Grey level means in the tumor and the aorta were plotted as a function of time during one hour. The analysis of the perfusion was performed using the program IRMA (developed in house) to assess the permeability rate (K_{trans}) and the plasmatic volume (Vp) of the tumor. These perfusion studies were performed in the same animal (n=5) at different stages of tumor growth: 5, 8, and 11/12 days after tumor induction.

2. In vivo biodistribution of Dotarem® and Gd-K

A group of 5 tumor-bearing mice was studied per contrast agent, at days 4 and 8 post tumor induction. A T_1-weighted spin echo sequence (resolution 234×234 μm^2, TE/TR = 16/500 ms) was set and an image was obtained each 32 seconds, for 1h15. The contrast agents Dotarem® or Gd-K were manually injected (100 µL; 0.2 mmol/kg) 4 min after the beginning of the acquisition via a catheter placed in the caudal vein. Grey level means in the tumor, muscle and kidneys were plotted as a function of time during one hour.

Ex vivo biodistribution studies

1. Radiolabeling of DOTA and K

$^{111}InCl_3$ was purchased from Mallinckrodt / Curiumpharma (Le Petten, Netherlands).

Radiolabeling of K and DOTA was performed as follows: 430 µL of a 22.4 µM solution of K was mixed with 125 µL of $^{111}InCl_3$ (130 MBq) and 125 µL NH_4OAc buffer (pH 5) or 220 µL of a 10.6 µM solution of DOTA was mixed with 70 µL of $^{111}InCl^3$ (73 MBq) and 70 µL NH_4OAc buffer (pH 5). Both solutions were stirred for 1h at 90°C. Labelling efficiency was followed by radio thin-layer chromatography (TLC). Radio TLCs were performed using silica gel IBF-2 Baker plates, and citrate buffer as mobile phase. The TLCs were measured on a miniGITA Star RadioTLC system (Elysia, Raytest, Belgium). In this TLC system, the radiocomplexes ^{111}In-K and ^{111}In-DOTA do not migrate (R_f = 0 – 0.1) while free ^{111}In has a R_f of 0.95. A radiochemical yield > 98% was obtained and no further purification was performed.

Prior to injection, the radiocomplex solutions were diluted with a PBS/saline buffer.

2. Ex vivo biodistribution studies

A group of six tumor bearing-mice per ligand and per murine model (tumor volume 60±10 mm^3) were injected intravenously (tail vein) with 7.5±1.5 MBq of ^{111}In-DOTA-K and 8.0±1.6 MBq of ^{111}In-DOTA (in 200µL) and an *ex vivo* biodistribution study was performed at 15 min and 4 h post-injection. After these time points, mice were sacrificed by cervical dislocation and the organs of interest (tumor, pancreas, brain, kidneys, lungs, heart, liver, spleen, intestine, muscle and bone (femur)) were harvested, weighted and their activity measured using a Carpintec gamma counter as well as a NaI based γ-camera (the acquired spectra are treated with WinTMCA program). Calibration of both equipment was done by measuring a set of 9 solutions

with activities between 0 and 1 MBq in both equipment, under the same conditions of the organs' measurements (distance and time and energy range of measurement acquisition). All data were corrected for the activity decay, bringing the activity to the injection time of each animal, as well as converted to MBq (Carpintec) using the calibration curve obtained. Biodistribution data are presented as % of injected dose per weight of organ (% ID/g±SEM, n=3).

A sample of the blood collected at the time of sacrifice was evaluated by TLC to assess the *in vivo* stability of the ^{111}In-K probe.

Acknowledgments

The authors acknowledge financial support from La Ligue Contre le Cancer (Comités du Loiret et des Deux Sèvres) and the Cancéropôle Grand Ouest (AOE 2020). The authors also thank Marilyne Le Mee, Stéphanie Retif and Rudy Clémençon for their contribution to the in vivo experiments and the MRI and TAAM-In vivo Imaging sub-platforms of the MO2VING facility (Orléans, France). SL thanks Dr Benjamin Gibert and Pr Patrick Mehlen for kindly providing the 4T1 cell line (overexpressing Netrin-1).

Supporting Information

Supporting Information: HPLC chromatograms and mass spectra of K and Rho-K; 3D representation of the molecular modeling and evolution plot of molecular dynamics, details on Fractional Occupation, MR images of Dotarem®, signal enhancement of Gd-K in the muscle, biodistribution profiles for ^{111}In-DOTA, complete ex-vivo biodistribution uptake data, and radio-TLC profile of a blood sample of a mouse injected with ^{111}In-K. This material is available free of charge via the Internet at http://pubs.acs.org/BC.

Abbreviations

DELFIA, Dissociation-enhanced lanthanide fluoroimmunoassays

DOTA, 1,4,7,10-Tetraazacyclododecane-1,4,7,10-tetraacetic acid

FOV, Field of View

ICP-OES, Inductively Coupled Plasma Optical Emission spectroscopy

MRI, Magnetic Resonance Imaging

NMRD, Nuclear Magnetic Relaxation Dispersion

PBS, Phosphate Buffered Saline

PET, Positron Emission Tomography

SPECT, Single Photon Emission Computed Tomography

TE, Echo time

TR, Repetition time

References

(1) Fares, J., Fares, M. Y., Khachfe, H. H., Salhab, H. A., and Fares, Y. (2020) Molecular principles of metastasis: a hallmark of cancer revisited. *Signal Transduct. Target Ther. 5*, 28.

(2) Chen, K., and Conti, P. S. (2010) Target-specific delivery of peptide-based probes for PET imaging. *Adv. Drug Deliv. Rev. 62*, 1005-1022.

(3) Pantel, A. R., and Mankoff, D. A. (2017) Molecular imaging to guide systemic cancer therapy: Illustrative examples of PET imaging cancer biomarkers. *Cancer Lett. 387*, 25-31.

(4) Lacerda, S. (2018) Targeted Contrast Agents for Molecular MRI. *Inorganics 6*, 129.

(5) Zhou, Z., Qutaish, M., Han, Z., Schur, R. M., Liu, Y., Wilson, D. L., and Lu, Z. R. (2015) MRI detection of breast cancer micrometastases with a fibronectin-targeting contrast agent. *Nat. Commun. 6*, 7984.

(6) Han, Z. Design and Evaluation of Novel Contrast Agents for MR Molecular Imaging of Cancer. PhD Thesis, Case Western Reserve University, Cleveland, OH, United States, 2017.

(7) Ayat, N. R., Vaidya, A., Yeung, G. A., Buford, M. N., Hall, R. C., Qiao, P. L., Yu, X., and Lu, Z.-R. (2019) Effective MR Molecular Imaging of Triple Negative Breast Cancer With an EDB-Fibronectin-Specific Contrast Agent at Reduced Doses. *Front. Oncol. 9*, 1351.

(8) Mehlen, P., and Guenebeaud, C. (2010) Netrin-1 and its dependence receptors as original targets for cancer therapy. *Curr. Opin. Oncol. 22*, 46-54.

(9) Paradisi, A., and Mehlen, P. (2010) Netrin-1, a missing link between chronic inflammation and tumor progression. *Cell Cycle 9*, 1253-1262.

(10) Sun, K. L. W., Correia, J. P., and Kennedy, T. E. (2011) Netrins: versatile extracellular cues with diverse functions. *Development 138*, 2153-2169.

(11) Delloye-Bourgeois, C., Fitamant, J., Paradisi, A., Cappellen, D., Douc-Rasy, S., Raquin, M. A., Stupack, D., Nakagawara, A., Rousseau, R., Combaret, V., et al. (2009) Netrin-1 acts as a survival factor for aggressive neuroblastoma. *J. Exp. Med. 206*, 833-847.

(12) Fitamant, J., Guenebeaud, C., Coissieux, M. M., Guix, C., Treilleux, I., Scoazec, J. Y., Bachelot, T., Bernet, A., and Mehlen, P. (2008) Netrin-1 expression confers a selective advantage for tumor cell survival in metastatic breast cancer. *Proc. Natl. Acad. Sci. U.S.A. 105*, 4850-4855.

(13) Kryza, D., Wischhusen, J., Richaud, M., Hervieu, M., Sidi Boumedine, J., Delcros, J. G., Besse, S., Baudier, T., Laval, P. A., Breusa, S., et al. (2023) From netrin-1-targeted SPECT/CT to internal radiotherapy for management of advanced solid tumors. *EMBO Mol. Med.*, e16732.

(14) Wischhusen, J., Wilson, K. E., Delcros, J.-G., Molina-Peña, R., Gibert, B., Jiang, S., Ngo, J., Goldschneider, D., Mehlen, P., Willmann, J. K., et al. (2018) Ultrasound molecular imaging as a non-invasive companion diagnostic for netrin-1 interference therapy in breast cancer. *Theranostics 8*, 5126-5142.

(15) Finci, L. I., Krüger, N., Sun, X., Zhang, J., Chegkazi, M., Wu, Y., Schenk, G., Mertens, H. D. T., Svergun, D. I., Zhang, Y., et al. (2014) The crystal structure of netrin-1 in complex with DCC reveals the bifunctionality of netrin-1 as a guidance cue. *Neuron 83*, 839-849.

(16) Cooper, M. S., Sabbah, E., and Mather, S. J. (2006) Conjugation of chelating agents to proteins and radiolabeling with trivalent metallic isotopes. *Nat. Protoc. 1*, 314-317.

(17) Kostelnik, T. I., and Orvig, C. (2019) Radioactive Main Group and Rare Earth Metals for Imaging and Therapy. *Chem. Rev. 119*, 902-956.

(18) De Silva, C. R., Vagner, J., Lynch, R., Gillies, R. J., and Hruby, V. J. (2010) Optimization of time-resolved fluorescence assay for detection of europium-tetraazacyclododecyltetraacetic acid-labeled ligand-receptor interactions. *Anal. Biochem. 398*, 15-23.

(19) Handl, H. L., Vagner, J., Yamamura, H. I., Hruby, V. J., and Gillies, R. J. (2005) Development of a lanthanide-based assay for detection of receptor–ligand interactions at the δ-opioid receptor. *Anal. Biochem. 343*, 299-307.

(20) Phinikaridou, A., Lacerda, S., Lavin, B., Andia, M. E., Smith, A., Saha, P., and Botnar, R. M. (2018) Tropoelastin: A novel marker for plaque progression and instability. *Circ. Cardiovasc. Imaging 11*, e007303.

(21) Chaher, N., Digilio, G., Lacerda, S., Botnar, R. M., and Phinikaridou, A. (2023) Optimized Methods for the Surface Immobilization of Collagens and Collagen Binding Assays. *J. Vis. Exp.*, e64720.
(22) Caravan, P., Cloutier, N. J., Greenfield, M. T., McDermid, S. A., Dunham, S. U., Bulte, J. W. M., Amedio, J. C., Looby, R. J., Supkowski, R. M., Horrocks, W. D., et al. (2002) The Interaction of MS-325 with Human Serum Albumin and Its Effect on Proton Relaxation Rates. *J. Am. Chem. Soc. 124*, 3152-3162.
(23) Overoye-Chan, K., Koerner, S., Looby, R. J., Kolodziej, A. F., Zech, S. G., Deng, Q., Chasse, J. M., McMurry, T. J., and Caravan, P. (2008) EP-2104R: A Fibrin-Specific Gadolinium-Based MRI Contrast Agent for Detection of Thrombus. *J. Am. Chem. Soc. 130*, 6025-6039.
(24) Agemy, L., Sugahara, K. N., Kotamraju, V. R., Gujraty, K., Girard, O. M., Kono, Y., Mattrey, R. F., Park, J.-H., Sailor, M. J., Jimenez, A. I., et al. (2010) Nanoparticle-induced vascular blockade in human prostate cancer. *Blood 116*, 2847-2856.
(25) Buchwald, P. (2019) A Receptor Model With Binding Affinity, Activation Efficacy, and Signal Amplification Parameters for Complex Fractional Response Versus Occupancy Data. *Front. Pharmacol. 10*, 605.
(26) Zhang, Y., and Sanner, M. F. (2019) AutoDock CrankPep: combining folding and docking to predict protein–peptide complexes. *Bioinformatics 35*, 5121-5127.
(27) Merbach, A. E., Helm, L., and Toth, E. (2013) *The Chemistry of Contrast Agents in Medical Magnetic Resonance Imaging*, second ed., John Wiley & Sons, Chichester.
(28) Yamamoto, A., Huang, Y., Krajina, B. A., McBirney, M., Doak, A. E., Qu, S., Wang, C. L., Haffner, M. C., and Cheung, K. J. (2023) Metastasis from the tumor interior and necrotic core formation are regulated by breast cancer-derived angiopoietin-like 7. *Proc. Natl. Acad. Sci. U.S.A. 120*, e2214888120.
(29) Arroyo-Crespo, J. J., Armiñán, A., Charbonnier, D., Deladriere, C., Palomino-Schätzlein, M., Lamas-Domingo, R., Forteza, J., Pineda-Lucena, A., and Vicent, M. J. (2019) Characterization of triple-negative breast cancer preclinical models provides functional evidence of metastatic progression. *Int. J. Cancer 145*, 2267-2281.
(30) Crich, S. G., Terreno, E., and Aime, S. (2017) Nano-sized and other improved reporters for magnetic resonance imaging of angiogenesis. *Adv. Drug Deliv. Rev. 119*, 61-72.
(31) Zhang, J., Winters, K., Kiser, K., Baboli, M., and Kim, S. G. (2020) Assessment of tumor treatment response using active contrast encoding (ACE)-MRI: Comparison with conventional DCE-MRI. *PLoS One 15*, e0234520.
(32) Yankeelov, T. E., and Gore, J. C. (2009) Dynamic Contrast Enhanced Magnetic Resonance Imaging in Oncology: Theory, Data Acquisition, Analysis, and Examples. *Curr. Med. Imaging Rev. 3*, 91-107.
(33) Dassin, E., Eberlin, A., Briere, J., Dosne, A. M., and Najean, Y. (1978) Metabolic fate of 111Indium in the rat. *Int. J. Nucl. Med. Biol. 5*, 34-37.
(34) Barge, A., Cravotto, G., Gianolio, E., and Fedeli, F. (2006) How to determine free Gd and free ligand in solution of Gd chelates. A technical note. *Contrast Media Mol. Imaging 1*, 184-188.
(35) Ravindranath, P. A., Forli, S., Goodsell, D. S., Olson, A. J., and Sanner, M. F. (2015) AutoDockFR: Advances in Protein-Ligand Docking with Explicitly Specified Binding Site Flexibility. *PLoS Comput. Biol. 11*, e1004586.
(36) Thévenet, P., Shen, Y., Maupetit, J., Guyon, F., Derreumaux, P., and Tufféry, P. (2012) PEP-FOLD: an updated de novo structure prediction server for both linear and disulfide bonded cyclic peptides. *Nucleic Acids Res. 40*, W288-W293.
(37) Shen, Y., Maupetit, J., Derreumaux, P., and Tufféry, P. (2014) Improved PEP-FOLD Approach for Peptide and Miniprotein Structure Prediction. *J. Chem. Theory Comput. 10*, 4745-4758.
(38) Pettersen, E. F., Goddard, T. D., Huang, C. C., Couch, G. S., Greenblatt, D. M., Meng, E. C., and Ferrin, T. E. (2004) UCSF Chimera—A visualization system for exploratory research and analysis. *J. Comput. Chem. 25*, 1605-1612.

(39) D.A. Case, I.Y. Ben-Shalom, S.R. Brozell, D.S. Cerutti, T.E. Cheatham III, V.W.D. Cruzeiro, T.A. Darden, R.E. Duke, D. Ghoreishi, M.K. Gilson, et al. AMBER 18. University of California, San Francisco, 2018.

(40) Wang, J., Wolf, R. M., Caldwell, J. W., Kollman, P. A., and Case, D. A. (2004) Development and testing of a general amber force field. *J. Comput. Chem. 25*, 1157-1174.

(41) Olsson, M. H., Søndergaard, C. R., Rostkowski, M., and Jensen, J. H. (2011) PROPKA3: Consistent Treatment of Internal and Surface Residues in Empirical pKa Predictions. *J. Chem. Theory Comput. 7*, 525-537.

(42) Maier, J. A., Martinez, C., Kasavajhala, K., Wickstrom, L., Hauser, K. E., and Simmerling, C. (2015) ff14SB: Improving the Accuracy of Protein Side Chain and Backbone Parameters from ff99SB. *J. Chem. Theory Comput. 11*, 3696-3713.

(43) Corsi, D. M., Platas-Iglesias, C., Bekkum, H. v., and Peters, J. A. (2001) Determination of paramagnetic lanthanide(III) concentrations from bulk magnetic susceptibility shifts in NMR spectra. *Magn. Reson. Chem. 39*, 723-726.

Table of Contents graphic (TOC) :